International Journal of Latest Engineering and Management Research (IJLEMR)
ISSN: 2455-4847
www.ijlemr.com || Volume 04 - Issue 04 || April 2019 || PP. 07-20

Numerical Analysis of the Stability of Cemented Backfill Sill Mats Using Discontinuity Layout Optimization

Zakaria Oulbacha,
M.Sc.A., M.Eng., MBA
Dept. of Civil, Geological and Mining Engineering, École Polytechnique de Montréal, Canada

Abstract: Cemented backfill is one of the most suitable solutions to improve ground control in underground mining operations and increase ore extraction rate. When the walls and ore bodies are of poor quality, underhand cut-and-fill mining is often adopted: upper ore levels are mined first, and ore sills between working levels are mined for their economic value and replaced by artificially built cemented backfill sill mats. A critical aspect is to assess the stability and required strength for such platforms. Analytical solutions to estimate the necessary strength of cemented backfill sill mats were proposed by Mitchell and are used in a conservative way by practitioners. In this paper, Discontinuity Layout Optimization (DLO), a new validated limit analysis numerical procedure for geotechnical stability assessment, was used to investigate the applicability and validity conditions of existing available analytical models. Numerical analyses allowed to highlight the limitations of the available analytical solutions. A new failure mode was generated numerically and a new analytical solution for the flexural failure mode was developed. A discussion follows for suggestions of improvements taking into account other factors that influence the stability of sill mats.
Keywords: Discontinuity Layout Optimization, Failure mode, Cemented backfill, Analytical model, Sill mat

I. INTRODUCTION

Mining operations produce large quantities of solid waste, mainly in the form of waste rock and tailings. The use of mine backfill can be a solution for the management of mine solid waste (Aubertin et al., 2002; Tesarik et al., 2003; Gauthier, 2004; Potvin & Thomas, 2005). Mine backfill is generally produced from solid waste, water and a binder. The practice of using mine backfill to fill mined stopes has gained an increased popularity over the past decade (Belem & Benzazouaa 2003; Benzazouaa et al., 2005; 2008). The main advantages of mine backfill include improving ground control, ore extraction rate and reducing ore dilution rate (Hassani & Archibald 1998; Fall et al., 2009).

When the walls and ore bodies are of poor quality, an underhand cut-and-fill mining method is often adopted (Helinski et al., 2011). In such cases, upper ore levels are often mined first, and the ore sill pillars between working levels are mined for their economic value and replaced by artificially built sill mats (Marcinyshin, 1996; Pakalnis et al., 2005; Donovan et al., 2007). Sill mats are often built using cemented mine backfill for practicality and serve to support the overlying unconsolidated fill and safely mine the stope underneath (Mitchell, 1991; Caceres, 2005; Caceres et al., 2007). In this sense, it is crucial to properly estimate the necessary strength of cemented backfill sill mats. An overestimation of the required strength will induce excessive cement use and can potentially hurt the profitability of mining operations. An underestimation of the required strength can lead to sill mat failure and consequently pose a serious hazard for personnel working underneath and damage equipment (Mitchell, 1991).

The only available analytical solutions to estimate the minimum required strength of unreinforced cemented mine backfill sill mats were proposed by Mitchell (1991). Few updates have been reported in the literature (e.g. Caceres, 2005; Caceres et al., 2007; Oulbacha, 2014). Moreover, Mitchell's (1991) analytical solutions are used by practitioners in a conservative way due to several simplifying hypotheses.

In this paper, the author first recalls the analytical model developed by Mitchell (1991) to evaluate the stability of cemented backfill sill mats. A series of numerical simulations was performed to investigate the applicability and validity conditions of the available analytical solutions for the design of unreinforced cemented backfill sill-mats. Failure mechanisms are investigated as a function of the geometry of sill mats, loading sand the geotechnical properties of the materials.

II. ANALYTICAL SOLUTIONS FOR CEMENTED BACKFILL SILL MAT DESIGN

By combining laboratory centrifuge test (Mitchell et al., 1982; Mitchell & Roettger, 1989) and limit equilibrium analyses, Mitchell (1991) concluded that four modes of failure can be involved in the stability of unreinforced cemented backfill sill mats. Fig. 1 shows Mitchell's (1991) model with a sill-mat supporting an overlying unconsolidated fill and subject to various stresses. L and d represent the width and thickness of the sill-mat respectively, β the stope dip, w the weight of the sill-mat, σ_t the tensile strength of the sill-mat, τ the shear strength along the sill mat-rock interface, σ_n the normal lateral confinement stress and σ_v the overlying vertical loading stress assumed uniformly distributed by Mitchell. The major failure modes considered by Mitchell are: sliding, flexural, rotational and caving.

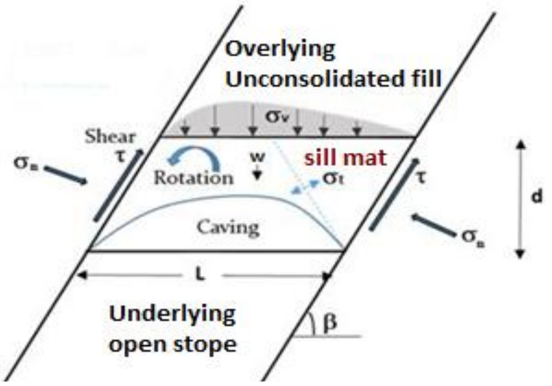

Figure 1: Illustration of a sill mat model supporting an overlying unconsolidated fill and subject to various stresses (Modified from Mitchell, 1991)

2.1. Sliding failure

Sliding failure occurs when the sill mat is thick and narrow. In this failure mode, the sill-mat slides along the interfaces as a rigid block. The following equation was proposed by Mitchell (1991) for the sliding failure mode:

$$\sigma_v + d\gamma > 2\left(\frac{\tau}{sin^2\beta}\right)\left(\frac{d}{L}\right) \quad (1)$$

Where, γ represents the unit weight of the sill mat.

2.2. Flexural failure

Flexural failure occurs when the sill-mat is wide and thin. In this failure mode, the sill mat flexes like a beam. By using standard formulae of uniformly loaded fixed beam, Mitchell (1991) proposed the following equation for the flexural failure mode:

$$\left(\frac{L}{d}\right)^2 > \frac{2\,(\sigma_t+\sigma_n)}{\sigma_v+\gamma d} \quad (2)$$

2.3. Rotational failure

Rotational failure occurs when the stope dip angle and the shearing resistance at the hanging wall contact are low. In this failure mode, the sill-mat detaches from the hanging wall and rotates relative to the footwall and falls under the effect of gravity. Mitchell (1991) proposed the following equation for the rotational failure mode:

$$\sigma_v + d\,\gamma > \frac{d^2\sigma_t}{2\,L\,(L-d\,cot\beta)sin^2\beta} \quad (3)$$

Caceres (2005) presented an updated form of this equation for rotational failure. From data of the Musselwhite mine, Caceres noted that the shearing strength at the hanging wall contact is not negligible. In his equation, Caceres (2005) incorporated the shear strength τ along the interface between the rock and hanging wall and an α coefficient ranging from 0 to 1 to describe the quality of contact. The equation proposed by Caceres (2005) for rotational failure is presented below:

$$\sigma_v + d\,\gamma > \frac{d^2\sigma_t+2\,\alpha\,\tau\,d\,L\,sin^2\beta}{L\,(L-d\,cot\beta)sin^2\beta} \quad (4)$$

2.4. Caving failure

Mitchell (1991) proposed the following equation for the rotational failure mode. Finally, Mitchell (1991) considered that the sill mat should be narrow and thick for caving failure mode to occur. The failure surface is assumed to be semi-circular and the proposed equation by Mitchell (1991) is presented below:

$$\frac{\pi\,\gamma}{8} > \frac{\sigma_t}{L} \quad (5)$$

III. NUMERICAL MODELING

3.1. Discontinuity Layout Optimization

Numerical modeling is a very useful tool to model geotechnical problems. Discontinuity Layout Optimization (DLO) is a fairly recent validated numerical limit analysis technology (Smith & Gilbert 2008; Lee et al., 2008; Clarke et al., 2010) that provides a powerful alternative to other numerical methods such as finite elements limit analysis (A Rashid et al., 2017; Smith et al., 2017). DLO has gained increased usage for a wide range of geotechnical problems including slope stability, foundations, reinforced soils, retaining walls, tunnels (Smith & Tatari 2016; Vahedifard, et al., 2016; A Rashid et al., 2017; Liang et al., 2017; Zhang et al., 2018; Bolbotowski et al., 2018; Fortunato et al., 2018; Zhou et al., 2018).

DLO uses an arrangement of discrete slip-lines in the failure field of a plane plasticity problem and allows to directly identify the critical failure mechanism and provides a factor of safety for any geotechnical problem (A Rashid et al. 2017). Rather than being formulated in terms of elements, DLO is typically presented in it primal kinematic form (Smith & Gilbert 2007) where a regular nodes square grid is typically used in the solution. Fig. 2 illustrates the basic stages involved in the Discontinuity Layout Optimization (DLO) analysis procedure.

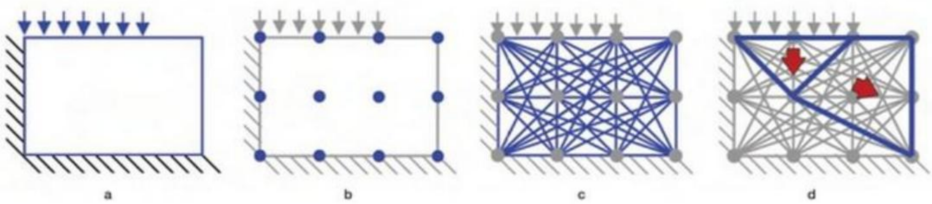

Figure 2: Basic stages of the DLO procedure: (a) Model initialization; (b) Discretization of the body using nodes; (c) Interconnection of nodes with potential discontinuities «slip-lines» horizontally, vertically and diagonally; (d) Optimization to identify the most critical failure mode (modified from LimitState 2019)

The first stage of the DLO procedure consists in an initialization of the model (Fig. 2a). During the second stage, a uniform meshing of the model is performed and the body is discretized using nodes (Fig. 2b). In the third stage, the nodes are interconnected horizontally, vertically and diagonally by potential lines of discontinuities "slip-lines" (Fig. 2c). In the fourth stage, an optimization procedure is used to identify the discontinuity lines that form the most critical mode of failure (Fig. 2d) and assess the stability of the problem using a factor of safety. It is interesting to note that the objective of the optimization process is to identify the minimum upper-bound solution represented by a subset of discontinuities that form the critical failure mode. Compared to the finite element method, the main advantage of the DLO procedure is the rapid and direct analysis of the state of failure, without excessive number of iterations during calculations. All possible failure modes are considered in the analysis, whether anticipated or not by the engineer, hence shortening the time necessary for stability analysis. Another advantage of DLO is that it gives numerically stable results, even if the problem is physically unstable. Currently, LimitState:GEO (LimitState, 2019) is the only commercially available software utilizing the DLO technology and is used for this study. Further detail of software validation and verification results are provided in LimitState (2019).

3.2. Conceptual Numerical Model

Fig. 3 illustrates a typical LimitState:GEO numerical model of sill mat with geometrical properties, material properties, contact interface properties and subject to normal stresses, as presented in the Mitchell (1991) model.

The rigid walls are fixed in the vertical direction but free in the horizontal direction to transfer the normal confinement stress σ_n to the sill mat. The sill mat is characterized by a density γ_s, a cohesion c_s, a friction angle ϕ_s and a tensile strength σ_t. The interfaces between rock walls and the sill mat are characterized by a cohesion c_i and a friction angle ϕ_i.

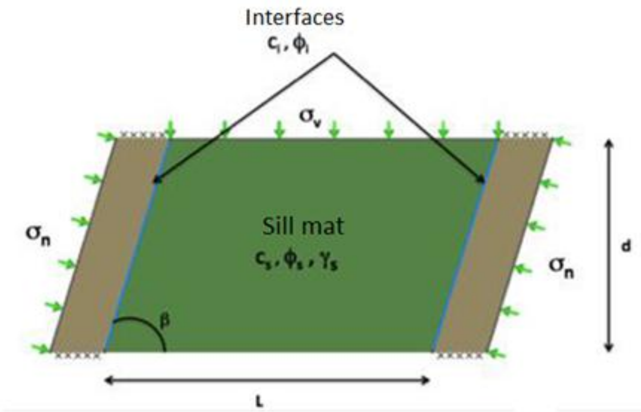

Figure 3: Typical numerical model of the sill mat with geometrical properties, material properties, contact interface properties and subject to normal stresses, using LimitState:GEO (adapted from Oulbacha, 2014)

For all numerical simulations, the density of the sill mat is fixed at a value of γ_s = 19 kN /m^3. The tensile strength of the sill-mat is calculated using to the Mohr-Coulomb criterion as follows:

$$\sigma_t = \frac{2\,c_s}{tan\left(45^\circ + \frac{\varphi_s}{2}\right)} \qquad (6)$$

IV. MAIN NUMERICAL RESULTS

4.1. Methodology

A numerical simulation program was considered for each failure mode. The simulation program was established from a reference case by varying one parameter at a time (geometries, material properties and loadings). Hence, a reference case study was chosen, simulated with the software and the parameters were modified until the failure mode observed numerically corresponded to the failure mode to be analyzed. Next, the numerical results were retained and compared to the corresponding analytical solutions. The values of parameters were chosen in a way to be representative of typical geometrical and geotechnical properties of cemented backfill sill mats as presented in the literature (Caceres, 2005; Pakalnis et al., 2005; Donovan et al., 2007; Caceres et al., 2007; Sobhi, 2014; Hughes, 2014).

4.2. Sliding failure analysis

Regarding sliding failure, Fig. 4 shows two typical cases of sliding failure obtained with the software LimitState: GEO for a vertical sill mat (Fig. 4a) and an inclined sill mat (Fig. 4b).

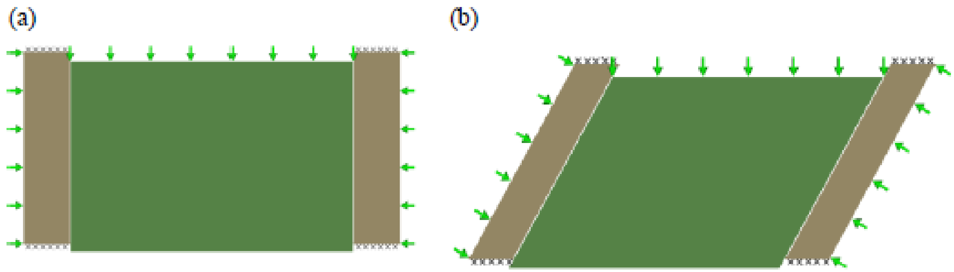

Figure 4: Typical sliding failure obtained with LimitState:GEO for (a) vertical sill mat β = 90° and (b) inclined sill mat β = 60°. Other parameters used are given in Table 1 (adapted from Oulbacha, 2014)

The simulation program used for sliding failure investigation is presented in Table 1. Figure 5 shows results of the variation of numerical and analytical of factors of safety (FS) versus sill mat width, L (Fig. 5a), sill mat thickness, d (Fig. 5b), sill mat cohesion c_s (Fig. 5c), sill mat friction angle ϕ_s (Fig. 5d), interface cohesion c_i (Fig. 5e), overlying vertical stress σ_v (Fig. 5f) and lateral normal confinement stress σ_n (Fig. 5g).

Table 1: Numerical simulation program of sliding failure (adapted from Oulbacha 2014)

	Geometry		Sill mat material		Interface	Normal Stresses	
Cases	L (m)	d (m)	C_s (kPa)	ϕ_s (°)	C_i (kPa)	σ_v (kPa)	σ_n (kPa)
Ref	6	4	1,500	35	50	200	1,000
Figure 5a	**Var**	4	1,500	35	50	200	1,000
Figure 5b	6	**Var**	1,500	35	50	200	1,000
Figure 5c	6	4	**Var**	35	50	200	1,000
Figure 5d	6	4	1,500	**Var**	50	200	1,000
Figure 5e	6	4	1,500	35	**Var**	200	1,000
Figure 5f	6	4	1,500	35	50	**Var**	1,000
Figure 5g	6	4	1,500	35	50	200	**Var**

As shown in Fig. 5, the analysis of sliding failure showed quasi-perfect correlations between the numerical and analytical results using the Mitchell (1991) solution. It is also interesting to mention that the same good correlations for sliding failure were obtained for other cases involving inclined stopes (see Oulbacha, 2014). Numerical results indicated that this type of failure mode is more conditioned by the rock-sill mat interface and the inclination of the sill mat, rather than the dimensions of the sill mat as claimed by Mitchell (1991). Numerical results showed that wide (10–16 m) and thin (1–2 m) sill mats were also subject to sliding failure, mainly due to the influence of the rock-sill mat interface properties. Hence, a sill mat is more likely to undergo sliding failure when the rock-sill mat interface is smooth and the stope is slightly inclined. It is therefore essential to be able to identify these properties in order to adequately predict and assess sliding failure.

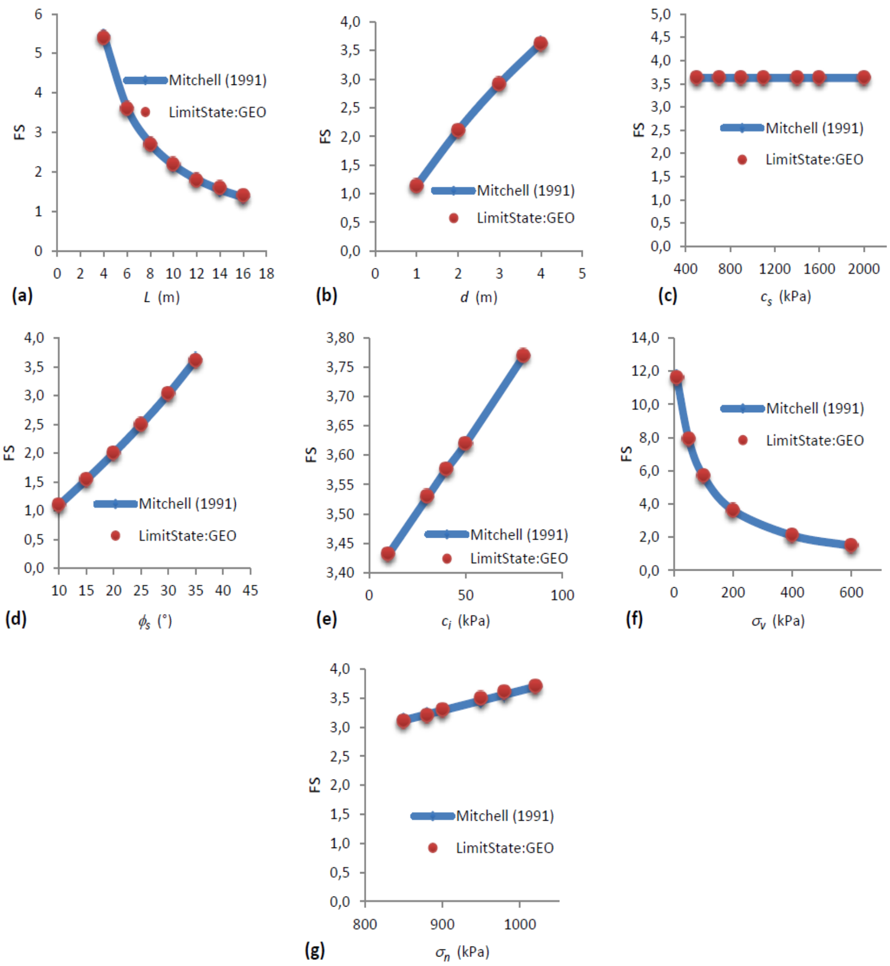

Figure 5: Numerical and analytical factors of safety (FS) versus (a) sill mat width *L* (b) sill mat thickness *d*, (c) and sill mat cohesion c_s, (d) sill mat friction angle ϕ_s, (e) interface cohesion ci,(f) overlying vertical stress σ_v, (g) lateral normal confinement stress σ_n; for a vertical stope with $\phi_i = \phi_s$. More details are given in Table 1 (adapted from Oulbacha, 2014)

4.3. Flexural failure analysis

Regarding flexural failure, Fig. 6 shows two typical cases of flexural failure obtained with the software LimitState: GEO for a vertical sill mat (Fig. 6a) and an inclined sill mat (Fig. 6b).

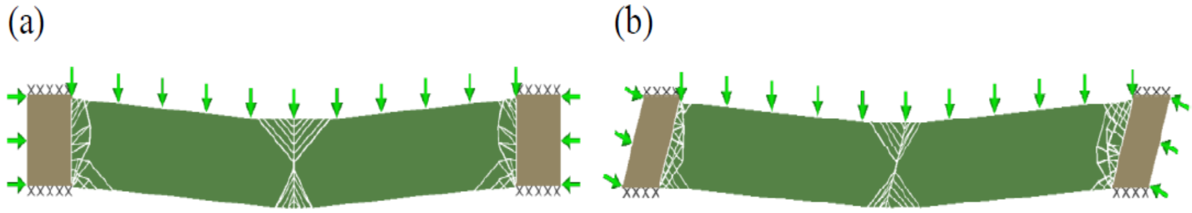

Figure 6: Typical flexural failure obtained with LimitState: GEO for (a) vertical sill mat β = 90° and (b) inclined sill mat β = 75°. Other parameters used are given in Table 2 (adapted from Oulbacha, 2014)

The simulation program used for flexural failure investigation is presented in Table 2. Fig.7 shows results of the variation of numerical and analytical of factors of safety (FS) versus sill mat width, *L* (Fig. 7a), sill mat thickness, *d* (Fig. 7b), sill mat inclination, β (Fig. 7c), sill mat cohesion c_s (Fig. 7d), sill mat friction angle ϕ_s (Fig. 7e), interface cohesion c_i (Fig. 7f), interface friction angle ϕ_i (Fig. 7g), overlying vertical stress σ_v (Fig. 7h) and lateral normal confinement stress σ_n (Fig. 7i).

Table 2: Numerical simulation program of flexural failure (adapted from Oulbacha, 2014)

	Geometry			Sill mat Material		Interface		Normal Stresses	
Cases	L (m)	d (m)	β (°)	C_s (kPa)	ϕ_s (°)	C_i (kPa)	ϕ_i (°)	σ_v (kPa)	σ_n (kPa)
Ref	10	1.5	90	1,500	35	1,300	35	150	1,000
Figure 7a	**Var**	1.5	90	1,500	35	1,300	35	150	1,000
Figure 7b	10	**Var**	90	1,500	35	1,300	35	150	1,000
Figure 7c	10	1.5	**Var**	1,500	35	1,300	35	150	1,000
Figure 7d	10	1.5	90	**Var**	35	1,300	35	150	1,000
Figure 7e	10	1.5	90	1,500	**Var**	1,300	35	150	1,000
Figure 7f	10	1.5	90	1,500	35	**Var**	35	150	1,000
Figure 7g	10	1.5	90	1,500	35	1,300	**Var**	150	1,000
Figure 7h	10	1.5	90	1,500	35	1,300	35	**Var**	1,000
Figure 7i	10	1.5	90	1,500	35	1,300	35	150	**Var**

Results through numerical modeling have shown that this failure mode can take place in vertical or inclined stopes up to 70° to the horizontal, for wide (10–14m) and thin (1–1.75m) sill mats. Discrepancies have been observed between the analytical and numerical results of Mitchell (1991). Stability is underestimated by the Mitchell (1991) analytical solution in all cases as shown in Fig. 7.

The divergence of results can be attributed to the fact that in the case of the analytical solution, as demonstrated by Oulbacha (2014), the model developed by Mitchell (1991) considered the maximum moment at both ends of a uniformly loaded clamped beam. However, since flexural failure occurs at the centre of the beam, the numerical model is developed in a way similar to a beam clamped on one end and free on the other while restricting rotation at both ends. In this case, the moment reaches its maximum at the centre where actual failure occurs and is zero at the edges of the sill mat.

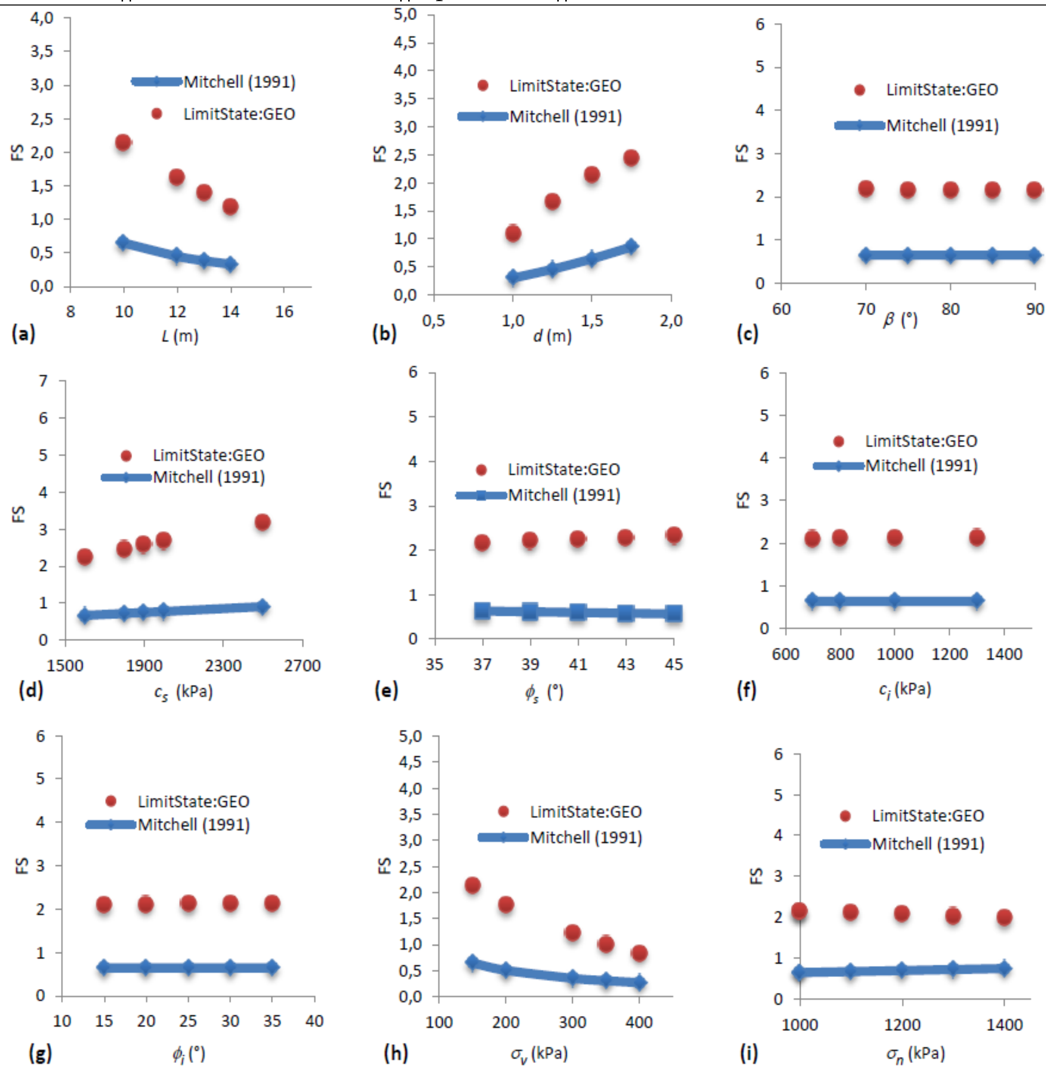

Figure 7: Numerical and analytical factors of safety (FS) versus (a) sill mat width L, (b) sill mat thickness d, (c) sill mat inclination β, (d) sill mat cohesion c_s ,(e) sill mat friction angle ϕ_s ,(f) interface cohesion c_i , (f) interface friction angle ϕ_i , (g) overlying vertical stress σ_v, (h) lateral normal confinement stress σ_n, (i); when flexural failure occurs. More details are given in Table 2 (adapted from Oulbacha, 2014)

In this sense, Oulbacha (2014) developed a new equation by considering the expression of the moment M at the centre of the beam. Flexural failure occurs at the centre of the beam, as the tensile strength is exceeded by tensile stress due to the moment at the centre. The equation developed by Oulbacha (2014) is shown below:

$$\sigma_{centre} = \frac{\left(\frac{(\sigma_v+\gamma d)\,L^2}{24}\right)\left(\frac{d}{2}\right)}{\frac{d^3}{12}} > \sigma_t + \sigma_n \qquad (7)$$

Or even: $\left(\frac{L}{d}\right)^2 > \frac{4\,(\sigma_t+\sigma_n)}{\sigma_v+\gamma d}$ (8)

The new equation is different from Mitchell's (1991) equation by a factor of 2 at the numerator. Fig. 8 shows a comparison of factors of safety (FS) obtained numerically and analytically with Oulbacha (2014) and Mitchell's (1991) equation.

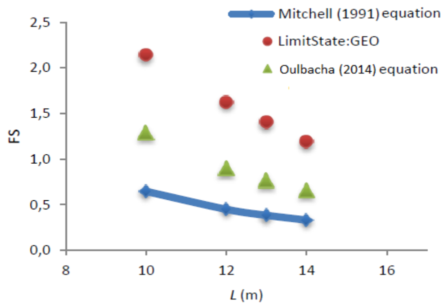

Figure 8: Comparison between numerical and analytical factors of safety (FS) using Mitchell and Oulbacha equations Vs. sill mat width *L*; when flexural failure occurs. Other parameters used are given in Table 2 (adapted from Oulbacha, 2014)

Results shown in Fig.8 indicate that by considering the stability of the beam at the centre, Oulbacha's new equation allows to describe slightly better the numerical results, as compared to the Mitchell (1991) solution. However, we can still observe that the new analytical solution still largely underestimates the stability of the sill-mat as compared to numerical results.

4.4. Rotational failure analysis

Regarding rotational failure, Oulbacha (2014) evaluated the validity of the analytical solutions of Mitchell (1991) and Caceres (2005) for this failure mode. Fig. 9 shows two typical cases of rotational failure obtained with the software LimitState: GEO for a 75° inclined sill mat (Fig. 9a) and a 50° inclined sill mat (Fig. 9b). We can observe that the upper left corner wedge of the sill mat has an effect of preventing rotation as it crushes against the rock wall. As the sill mat inclination increases (Fig. 9b), rotation occurs more easily as the size of the upper left corner wedge decreases since it crushes less against the wall.

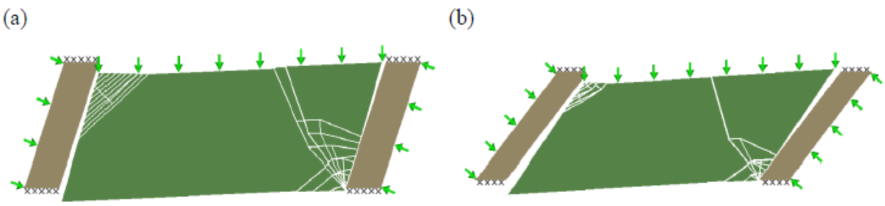

Figure 9: Typical rotational failure obtained with LimitState: GEO for (a) β = 75° inclined sill mat and (b) β = 50° inclined sill mat. Other parameters used are given in Table 3 (adapted from Oulbacha, 2014)

The simulation program used for rotational failure investigation is presented in Table 3. Fig. 10 shows results of the variation of numerical and analytical of factors of safety (FS) versus sill mat width, *L* (Fig. 10a), sill mat thickness, *d* (Fig. 10b), sill mat inclination, *β* (Fig. 10c), sill mat cohesion c_s (Fig. 10d), sill mat friction angle ϕ_s (Fig. 10e), interface cohesion c_i (Fig. 10f), interface friction angle ϕ_i (Fig. 10g), overlying vertical stress σ_v (Fig. 10h) and lateral normal confinement stress σ_n (Fig. 10i).

Table 3: Numerical simulation program of rotational failure (adapted from Oulbacha, 2014)

Cases	Geometry			Sill mat Material		Interface		Normal Stresses	
	L (m)	d (m)	β (°)	C_s (kPa)	ϕ_s (°)	C_i (kPa)	ϕ_i (°)	σ_v (kPa)	σ_n (kPa)
Ref	8	3	70	2,500	35	150	35	250	1,400
Figure 10a	**Var**	3	70	2,500	35	150	35	250	1,400
Figure 10b	8	**Var**	70	2,500	35	150	35	250	1,400
Figure 10c	8	3	**Var**	2,500	35	150	35	250	1,400
Figure 10d	8	3	70	**Var**	35	150	35	250	1,400
Figure 10e	8	3	70	2500	**Var**	150	35	250	1,400
Figure 10f	8	3	70	2,500	35	**Var**	35	250	1,400
Figure 10g	8	3	70	2,500	35	150	**Var**	250	1,400
Figure 10h	8	3	70	2,500	35	150	35	**Var**	1,400
Figure 10i	8	3	70	2,500	35	150	35	250	**Var**

The general trend observed is that better correlations are obtained between the analytical solution of Caceres (2005) and numerical results when the sill mat inclination is set around 70°. When shifting the inclination from 70° (Fig. 10c), we can observe that the analytical solution of Caceres (2005) overestimates the stability when inclination is less than 70° and overestimates it when inclination is more than 70°. Moreover, the analytical solution of Caceres (2005) predicts a deterioration of stability of the sill mats as the stope inclination increases, while an inverse trend is observed by numerical results (Fig. 10c). Moreover, numerical modeling with LimitState: GEO visually shows this trend (Fig. 10b) when the higher the stope inclination, the easier rotation occurs, as the size of the upper left corner wedge decreases since it crushes less against the wall. This results in sill-mat stability reduction as inclination gets higher. Future work is therefore needed to improve the analytical solution of Caceres (2005) for the rotational failure.

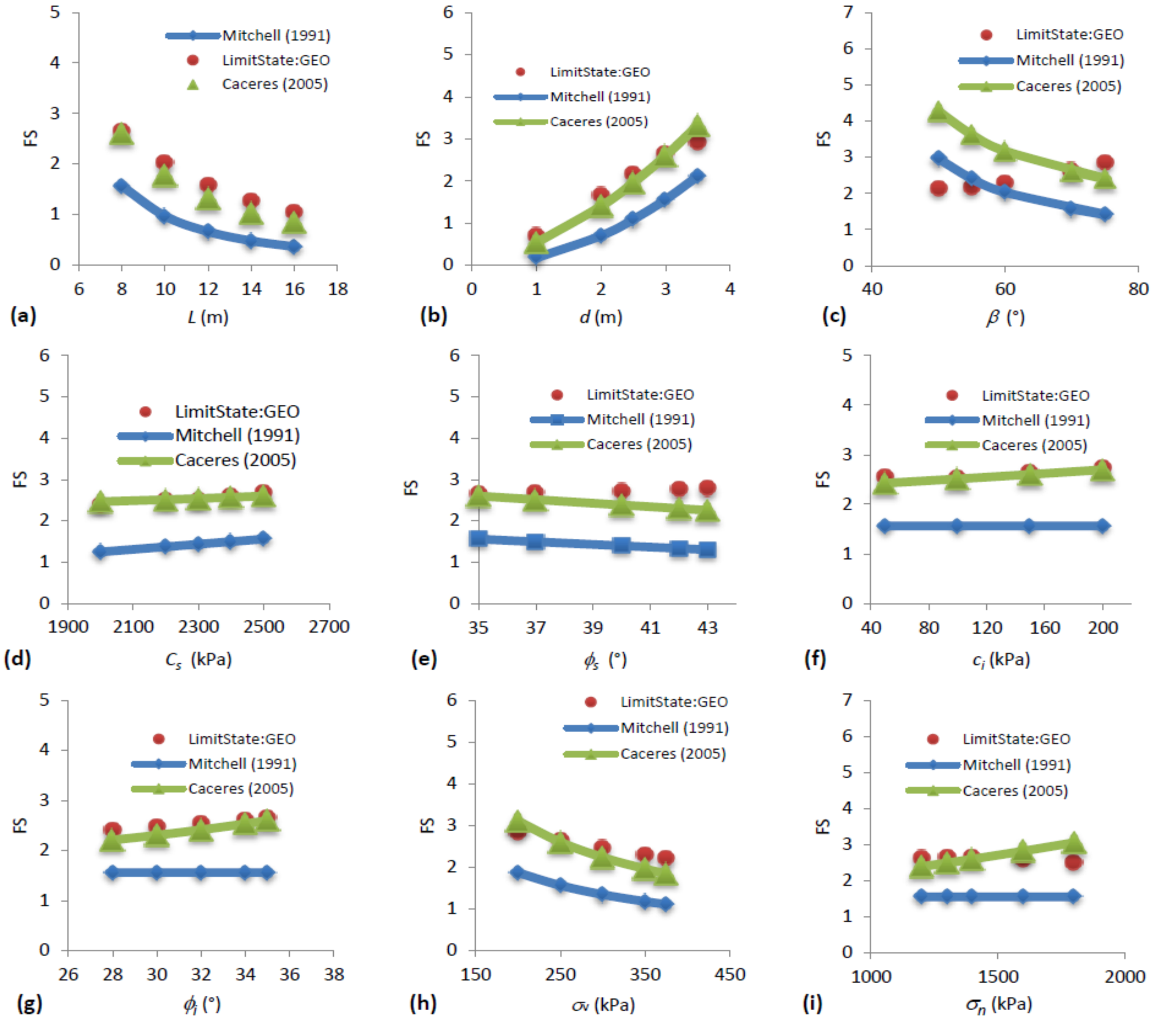

Figure 10: Numerical and analytical factors of safety (FS) versus (a) sill mat width L, (b) sill mat thickness d, (c) sill mat inclination β, (d) sill mat cohesion c_s ,(e) sill mat friction angle ϕ_s ,(f) interface cohesion c_i , (f) interface friction angle ϕ_i , (g) overlying vertical stress σ_v, (h) lateral normal confinement stress σ_n, (i); when rotational failure occurs. More details are given in Table 3 (adapted from Oulbacha, 2014)

4.5. Caving failure analysis

Regarding caving failure, Fig. 11 shows two typical cases of caving failure obtained with the software LimitState: GEO for a low-resistance sill mat (Fig. 11a) and high-resistance sill mat (Fig. 11b).

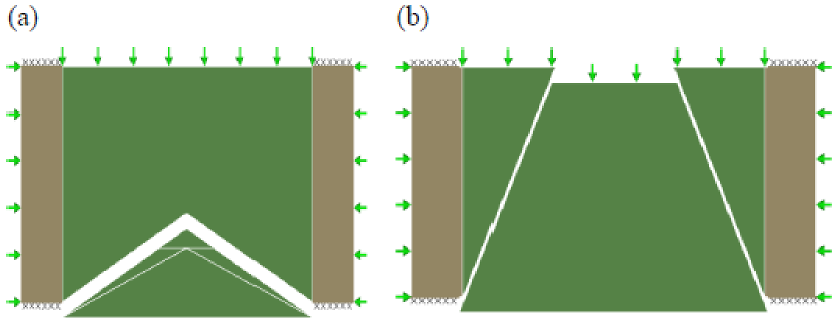

Figure 11: Typical caving failure obtained with LimitState: GEO for (a) low-resistance sill mat c_s=10 kPa and (b) high-resistance sill mat c_s=1500 kPa; when caving failure occurs. Other parameters used are given in Table 4 (adapted from Oulbacha 2014)

In comparison with the Mitchell (1991) model, we can observe that failure surfaces are not circular. When the resistance of the sill mat is low, we can observe a block detaching from underneath (Fig. 11a) as expected by Mitchell for caving failure. When the resistance of the sill mat is high, we can observe caving failure of a block shearing through the sill mat (Fig. 11b). This caving failure was not predicted in the Mitchell (1991) model. Fig. 12 shows that the Mitchell (1991) solution assesses stability fairly well for low-cohesion sill mats. However, as the sill-mat gains higher resistance (cohesion), Mitchell's (1991) analytical solution for caving failure tends to overestimate the stability of the sill mat as shown in Fig. 12. The simulation program used for caving failure investigation is presented in Table 4.

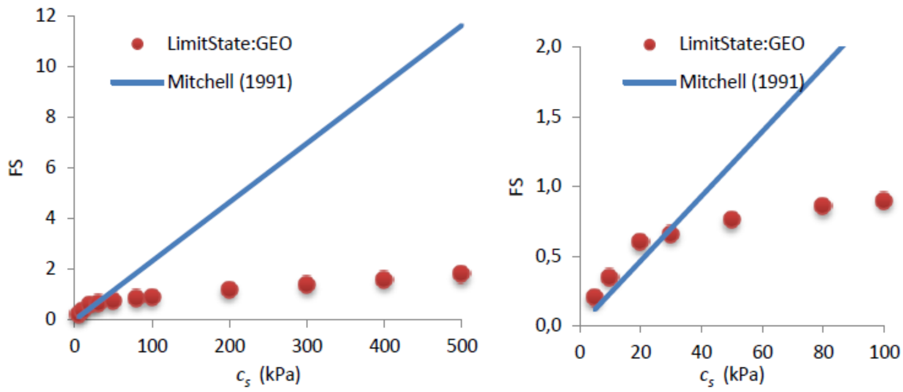

Figure 12: Numerical and analytical factors of safety Vs. sill mat cohesion c_s (left: normal scale; right: enlarged scale); when caving failure occurs. Other parameters used are given in Table 4 (adapted from Oulbacha 2014)

Table 4: Numerical simulations program of caving failure (adapted from Oulbacha 2014)

	Geometry			Sill mat Material		Interface		Normal Stresses	
Cases	L (m)	d (m)	β (°)	C_s (kPa)	$\square_s$ (°)	C_i (kPa)	$\square_i$ (°)	σ_v (kPa)	σ_n (kPa)
Ref	6	4	90	1,500	35	1,500	35	600	1,000
Figure 13a	**Var**	4	90	1,500	35	1,500	35	600	1,000
Figure 13b	6	**Var**	90	1,500	35	1,500	35	600	1,000
Figure 13c	6	4	**Var**	1,500	35	1,500	35	600	1,000
Figure 13d	6	4	90	**Var**	35	1,500	35	600	1,000
Figure 13e	6	4	90	1,500	**Var**	1,500	35	600	1,000
Figure 13f	6	4	90	1,500	35	**Var**	35	600	1,000
Figure 13g	6	4	90	1,500	35	1,500	**Var**	600	1,000
Figure 13h	6	4	90	1,500	35	1,500	35	**Var**	1,000
Figure 13i	6	4	90	1,500	35	1500	35	600	**Var**

Fig. 13 shows results of the variation of numerical and analytical of factors of safety (FS) versus sill mat width, L (Fig. 13a), sill mat thickness, d (Fig. 13b), sill mat inclination, β (Fig. 13c), sill mat cohesion c_s (Fig. 13d), sill mat friction angle ϕ_s (Fig. 13e), interface cohesion c_i (Fig. 13f), interface friction angle ϕ_i (Fig. 13g), overlying vertical stress σ_v (Fig. 13h) and lateral normal confinement stress σ_n (Fig. 13i). Results indicate in all cases that the Mitchell (1991) analytical solution overestimates the stability of sill mats. This overestimation could be explained by the high tensile strength gained from high cohesions (1,500–1,800 kPa) using the Mohr-Coulomb criterion. Since the Mitchell (1991) analytical factor of safety (FS) is proportional to the tensile strength, it tends to highly increase linearly as sill mat cohesion increases (Fig. 13d).

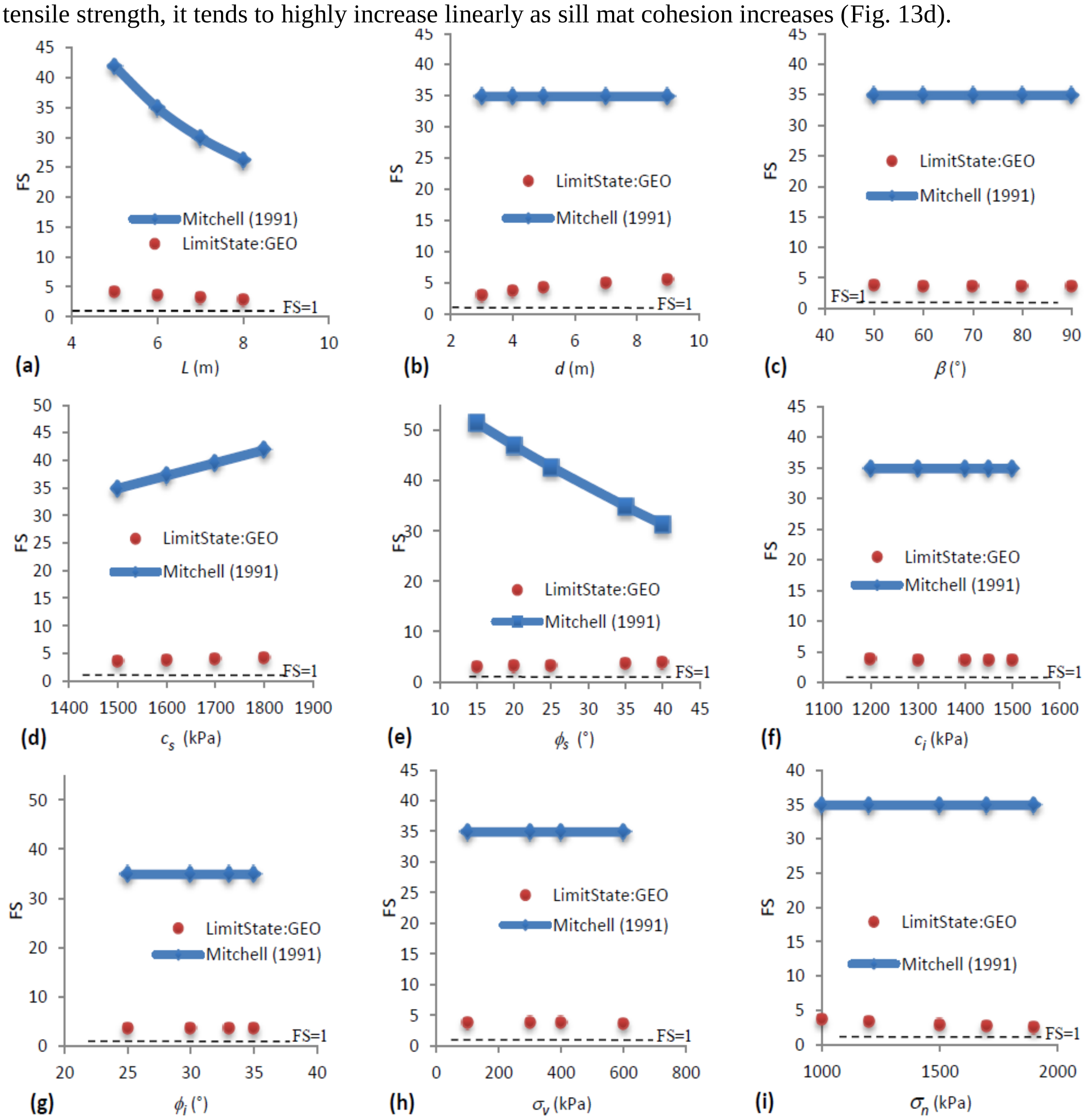

Figure 13: Numerical and analytical factors of safety (FS) versus (a) sill mat width L, (b) sill mat thickness d, (c) sill mat inclination β, (d) sill mat cohesion c_s ,(e) sill mat friction angle ϕ_s ,(f) interface cohesion c_i , (f) interface friction angle ϕ_i , (g) overlying vertical stress σ_v, (h) lateral normal confinement stress σ_n, (i); when caving failure occurs. More details are given in Table 4 (adapted from Oulbacha, 2014)

V. DISCUSSION

Firstly, it has been noted that the Mitchell (1991) model has several limitations, which have also been inherited in numerical modeling. For instance, Mitchell considered an isolated stope without taking into account adjacent excavations. Rock walls were assumed to be rigid and the depth of the stope was neglected. Some parameters used in Mitchell's analytical solutions remain unknown, such as the shear strength along rock walls τ or the normal confinement stress σ_n.

No equation has been proposed by Mitchell to determine these parameters. Another limitation is the consideration of rigid walls as in the Mitchell model. The mining and backfilling sequence of stopes above and below the sill mat were also totally neglected by Mitchell. Recent studies have shown that the backfilling sequence significantly impacts the stress distribution on sill mats (Sobhi 2014; Sobhi & Li, 2015).

Another limitation of this study is the use of the Mohr-Coulomb criterion to compute the tensile strength of the sill-mat via the cohesion and friction angle. This failure criterion is commonly used in geotechnical engineering, mainly for its simplicity. It is commonly known that the Mohr-Coulomb criterion is not representative of the behavior of materials with cohesion, such as rocks, concretes and cemented mineral fillings. It neglects the influence of the intermediate principal stress and tends to overestimate the resistance of materials with high confining pressure. More work is needed to take into account a more representative criterion for the study of sill-mat stability.

Another limitation of the analyses performed is that distribution of the overlying vertical stress on the sill-mat has been applied uniformly as considered in the Mitchell (1991) model. However, some studies have shown that this distribution is non-uniform due to the arching effect (Belem et al., 2005; Li & Aubertin 2008, 2010; Ting et al., 2011; Thompson et al., 2012). More work is needed to analyze the influence of a more realistic vertical stress distribution on sill-mat stability.

Moreover, the LimitState:GEO software also has certain limitations. For instance, the DLO procedure does not provide information on strains and the stress state before failure. In addition, the DLO procedure provides upper-bound solutions, which may sometimes underestimate the factor of safety and give non-conservative results (Es-Saheb et al., 2013).

VI. CONCLUSION

Numerical analyses of the stability of cemented backfill sill mats were conducted using the LimitState: GEO software and allowed to investigate the existing available analytical models for stability assessment and design. Results showed that Mitchell solutions do not correctly assess stability of sill mats for all four failure modes. The sliding failure analytical solution was validated. For flexural failure, the analytical solution was not validated as it underestimates stability due to simplifying hypotheses. A new equation for this failure mode was developed by the author and showed slightly better stability assessment as compared to the Mitchell (1991) solution. Regarding rotational failure, both the Mitchell (1991) solution and Caceres (2005) updated solution were assessed. Results showed that the Mitchell (1991) solution overall underestimates stability, while the Caceres (2005) solution provided good correlations with numerical results, when stope inclination was set around 70°. However, when shifting from this inclination, numerical results describe deteriorated stability with an inclination increase as explained before, while an opposite tendency is observed using the Caceres (2005) solution. For caving failure, the Mitchell (1991) solution assesses stability fairly well for low-cohesion sill-mats. However, for high-cohesion sill mats, the Mitchell (1991) solution largely overestimates stability. Moreover, a new caving failure mode unpredicted by Mitchell was generated through numerical modeling. This study helped to highlight the limitations of existing analytical solutions for cemented backfill sill mat design, provide guidance for improvement, and highlight the importance of numerical analysis assistance for sill-mat stability assessment and design. It is recommended for further research to use DLO to explore the behaviour of an actual sill mat and compare with field results.

.

VII. ACKNOWLEDGEMENTS

The author acknowledges the financial support from the Natural Sciences and Engineering Research Council of Canada (NSERC), the Institut de recherche Robert-Sauvé en Santé et en Securité du travail (IRSST) and the industrial partners of the Research Institute on Mines and Environment (RIME UQAT-Polytechnique).

REFERENCES

[1] Aubertin, M., Bernier, L. & Bussière, B. (2002). Environnement et gestion des rejets miniers. (CD-ROM), Presses internationals Polytechnique.

[2] A Rashid, A. S., Black, J. A., Kueh, A. B. H., Mohamad, H., & Md Noor, N. (2017). Bearing capacity charts of soft soil reinforced by deep mixing. *Proceedings of the Institution of Civil Engineers-Ground Improvement*, 170(1), pp. 12-25.

[3] Belem, T., Benzaazoua, M., & Bussière, B. (2003, February). Utilisation du remblai en pâte comme support de terrain. Partie I : De sa fabrication à La mise en place sous terre. In Symp. int. Apres-mines, GISOS, Gisos ed., Nancy, France (pp. 5-7).

[4] Belem, T., Fall, M., Aubertin, M. & Li, L.(2005). Développement d'une méthode intégrée d'analyse de stabilité des chantiers miniers remblayés. *Preliminary report, IRSST project*, 28.

[5] Benzaazoua, M., Bois, D., Belem, T., Gauthier, P., Ouellet, S., Fall, M. & St-Onge, J.F. (2005, March). Remblais souterrains, évolution des connaissances et de la pratique. *In 20th Colloque Contrôle de terrains*.

[6] Benzaazoua, M., Bussière, B., Demers, I., Aubertin, M., Fried, É. & Blier, A. (2008). Integrated mine tailings management by combining environmental desulphurization and cemented paste backfill: Application to mine Doyon, Quebec, Canada. *Minerals engineering*, 21(4), pp.330-340.https://doi.org/10.1016/j.mineng.2007.11.012

[7] Bolbotowski, K., He, L., & Gilbert, M. (2018). Design of optimum grillages using layout optimization. *Structural and Multidisciplinary Optimization*, 1-18

[8] Caceres, C. (2005). Effect of delayed backfill on open stope mining methods (Doctoral dissertation, University of British Columbia).

[9] Caceres, C., Pakalnis, R., Hughes, P. & Brady, T. (2007, January). Numerical modeling approach of failure modes for cemented backfill sill mats. *In 1st Canada-US Rock Mechanics Symposium. American Rock Mechanics Association*.

[10] Caceres, C., Moffat, R., & Pakalnis, R. (2017). Evaluation of flexural failure of sill mats using classical beam theory and numerical models. *International Journal of Rock Mechanics and Mining Sciences*, 99, pp. 21-27.

[11] Clarke, S. D., Smith, C. C., & Gilbert, M. (2010, May). Analysis of the stability of sheet pile walls using Discontinuity Layout Optimization. *In Proc. 7th Eur. Conf. Numer. Methods Geotech. Eng.(NUMGE), Trondheim, Norway* (pp. 163-168).

[12] Donovan, J., Dawson, J., & Bawden, W. F. (2007, April). David Bell Mine underhand cut and fill sill mat test. *In Proceedings of the 9th International Symposium in Mining with Backfill*, Montréal, Que (Vol. 29).

[13] Es-Saheb, M., Al-Witry, A., & Albedah, A. (2013). Analyses of plane-strain compression using the upper bound method. *Research Journal of Applied Sciences, Engineering and Technology*, 6(5), pp. 761-767. https://doi.org/10.19026/rjaset.6.4116

[14] Fall, M., Adrien, D., Celestin, J.C., Pokharel, M. & Toure, M. (2009). Saturated hydraulic conductivity of cemented paste backfill. *Minerals Engineering*, 22(15), 1307-1317.

[15] Fortunato, A., Fabbrocino, F., Angelillo, M., & Fraternali, F. (2018). Limit analysis of masonry structures with free discontinuities. *Meccanica*, *53*(7), pp. 1793-1802.

[16] Gauthier, P. (2004). Valorisation des liants et des rejets industriels dans les remblais miniers (DESS Thesis, Université du Québec en Abitbi-Témiscamingue).

[17] Gilbert, M., Smith, CC., Haslam, IW, & Pritchard, TJ. (2009). Plastic limit analysis using discontinuity layout optimization (DLO). *In 17th UK Conference on Computational Mechanics ACME-UK, Nottingham*.

[18] Hassani, F., & Archibald, J.(1998). Mine backfill. *Canadian Institute of Mining, Metallurgy and Petroleum, Montreal. (CD-ROM).*

[19] Hawksbee, S., Smith, C., & Gilbert, M. (2013). Application of discontinuity layout optimization to three-dimensional plasticity problems. *Proceedings of the Royal Society A: Mathematical, Physical and Engineering Sciences*, 469(2155), 20130009.

[20] Helinski, M., Fahey, M. & Fourie, A. (2010). Behavior of cemented paste backfill in two mine stopes: measurements and modeling. *Journal of geotechnical and geo-environmental engineering*, 137(2), pp.171-182. https://doi.org/10.1061/(asce)gt.1943-5606.0000418

[21] Hughes, P. B. (2014). Design guidelines: underhand cut and fill cemented paste backfill sill beams (Doctoral dissertation, University of British Columbia).

[22] Lee, Y., Smith, C. & Cheuk, C. Y. (2008). Bearing capacity of embedded foundations. *2nd International Conference on Foundations*, p. 961–972, ICOF, Dundee.

[23] Liang, T., & Knappett, J. A. (2017). Newmark sliding block model for predicting the seismic performance of vegetated slopes. *Soil Dynamics and Earthquake Engineering*, 101, pp. 27-40.

[24] Li, L. & Aubertin, M. (2008). An improved analytical solution to estimate the stress state in subvertical backfilled stopes. *Canadian Geotechnical Journal*, 45(10), pp.1487-1496.

[25] Li, L. & Aubertin, M. (2010). An analytical solution for the nonlinear distribution of effective and total stresses in vertical backfilled stopes. *Geomechanics and Geoengineering*, 5(4), pp.237-245.

[26] LimitState (2019). LimitState:GEO Validation- Verification results. Retrieved from http://www.limitstate.com/geo/validation

[27] Marcinyshyn, K.W. (1996). Sill mat design for narrow vein mining (Doctoral dissertation, University of British Columbia).

[28] Mitchell, R. J., Olsen, R. S., & Smith, J. D. (1982). Model studies on cemented tailings used in mine backfill. *Canadian Geotechnical Journal*, 19(1), 14-28. https://doi.org/10.1139/t82-002

[29] Mitchell, R., & Roettger, J. (1989). Analysis and modelling of sill pillars. Innovations in mining backfill technology. *Balkema, Rotterdam*, pp. 53-62.

[30] Mitchell, R. J.(1991). Sill mat evaluation using centrifuge models. Mining Science and Technology, 13(3), pp. 301-313.

[31] Oulbacha, Z.(2014). Analyse numérique de la stabilité des piliers-dalle en remblai cimenté : une vérification des modèles de Mitchell (Master's thesis, École Polytechnique de Montréal, Montreal, Canada).

[32] Pakalnis, R., Caceres, C., Clapp, K., Morin, M., Brady, T., Williams, T. & MacLaughlin, M. (2005). Design spans-underhand cut and fill mining. *Proceedings of 107th CIM-AGM, Toronto*.

[33] Potvin, Y., & Thomas, E. (2005). Handbook on mine fill.*Australian Centre for Geomechanics*.

[34] Smith, C. &Gilbert, M. (2007, October). Application of discontinuity layout optimization to plane plasticity problems. *In Proceedings of the Royal Society of London A: mathematical, physical and engineering sciences*. 463(2086), pp. 2461-2484. https://doi.org/10.1098/rspa.2006.1788

[35] Smith, C. & Gilbert, M.(2008). Limit analysis of the stability of foundations on inclined ground. *2nd International Conference on Foundations, ICOF 2008, Dundee*, p. 1683–1692.

[36] Smith, C. C., & Tatari, A. (2016). Limit analysis of reinforced embankments on soft soil. *Geotextiles and Geomembranes*, 44(4), 504-514.

[37] Smith, C. C., Gonzalez-Castejon, J., & Charles, J. (2017, September). Enhanced interpretation of geotechnical limit analysis solutions using Discontinuity Layout Optimization. *In 19th International Conference on Soil Mechanics and Geotechnical Engineering*, pp. 851-854. ASSMGE.

[38] Sobhi, M.A.(2014). Analyse numérique visant l'évaluation du coefficient de pression des terres et des contraintes dans des chantiers remblayés au-dessus d'un pilier-dalle (Master's thesis, École Polytechnique de Montréal, Montreal, Canada).

[39] Sobhi, M.A. & Li, L. (2015, January). A numerical study of the stresses in backfilled stopes overlying a sill mat. *In 13th ISRM International Congress of Rock Mechanics. International Society for Rock Mechanics and Rock Engineering*.

[40] Tesarik, D.R., Seymour, J.B. & Jones, F.M. (2003, January). Determination of in situ deformation modulus for cemented rockfill. *In 10th ISRM Congress. International Society for Rock Mechanics*.

[41] Thompson, B.D., Bawden, W.F. &Grabinsky, M.W. (2012). In situ measurements of cemented paste backfill at the Cayeli Mine. *Canadian Geotechnical Journal*, 49(7), pp.755-772. https://doi.org/10.1139/t2012-040

[42] Ting, C.H., Shukla, S.K. &Sivakugan, N. (2010). Arching in soils applied to inclined mine stopes. *International Journal of Geomechanics*, 11(1), pp.29-35. https://doi.org/10.1061/(ASCE)GM.1943-5622.0000067

[43] Vahedifard, F., Leshchinsky, D., Mortezaei, K., & Lu, N. (2016). Effective stress-based limit-equilibrium analysis for homogeneous unsaturated slopes. *International Journal of Geomechanics*, 16(6), D4016003.

[44] Zhou, H., Zheng, G., Yin, X., Jia, R. and Yang, X. (2017). The bearing capacity and failure mechanism of a vertically loaded strip footing placed on the top of slopes. *Computers and Geotechnics*, 94, pp.12-21. https://doi.org/10.1016/j.compgeo.2017.08.009

[45] Zhang, Y., Zhuang, X., & Lackner, R. (2018). Stability analysis of shotcrete supported crown of NATM tunnels with discontinuity layout optimization. *International Journal for Numerical and Analytical Methods in Geomechanics*, *42*(11), pp. 1199-1216.